Please cite as: D. Corinti, C. Coletti, N. Re, B. Chiavarino, M. E. Crestoni, S. Fornarini, *Chem. Eur. J.* **2016**, *22*, 3794.

Cisplatin Binding to Biological Ligands Revealed at the Encounter Complex Level by IR Action Spectroscopy

Davide Corinti,[a] Cecilia Coletti,[b] Nazzareno Re,[b] Barbara Chiavarino,[a] Maria Elisa Crestoni,[a] and Simonetta Fornarini*[a]

[a]*Dr. D. Corinti, Prof. B. Chiavarino, Prof. M. E. Crestoni, Prof. S. Fornarini*
Dipartimento di Chimica e Tecnologie del Farmaco, Università degli Studi di Roma La Sapienza, P.le A. Moro 5, I-00185 Roma, Italy. E-mail: simonetta.fornarini@uniroma1.it

[b]*Prof. C. Coletti, Prof. N. Re Dipartimento di Farmacia, Università G. D'Annunzio, Via dei Vestini 31, I-66100 Chieti, Italy.*

Supporting information for this article is available

Abstract. Cisplatin [*cis*-diamminedichloroplatinum(II)] is the first platinum-based antineoplastic agent and still a cornerstone for the treatment of various solid tumors. Reactive events responsible for cisplatin activity are unveiled here at the molecular level. Simple ligands (L) representing ubiquitous functional groups in the biological environment faced by the cisplatin drug are allowed to react with *cis*- $[PtCl(NH_3)_2(H_2O)]^+$, the primary intermediate from cisplatin hydrolysis, extracted from solution by electrospray ionization (ESI) and isolated in the gas phase. The kinetics and thermodynamics of the substitution reaction are examined by a combined experimental and computational approach and the structural features of the substitution product, *cis*-$[PtCl(NH_3)_2(L)]^+$, are probed by IR multiple photon dissociation (IRMPD) spectroscopy. Furthermore, IRMPD spectroscopy is exploited to disclose the structure of $[PtCl(NH_3)_2(L)(H_2O)]^+$ clusters, also delivered by ESI from the aqueous solution and representing the major focus of this investigation. These ions conform to a four-coordinate Pt(II) complex associated with an 'external' L molecule, namely the encounter complex of *cis*-$[PtCl(NH_3)_2(H_2O)]^+$ with the incoming ligand and represent the first direct evidence of a prototypical

Eigen-Wilkins encounter complex in solution, lying on the reaction coordinate for ligand substitution and extracted by ESI for mass spectrometric analysis. $[PtCl(NH_3)_2(L)(H_2O)]^+$ ions, activated by energetic collisions or by IR multiple photon absorption, dissociate by loss of either H_2O or L. The former process implies a ligand substitution event occurring within the activated cluster. IRMPD spectroscopy has thus revealed both structural details and reaction dynamics at the level of the isolated encounter complex.

Introduction

Cisplatin (*cis*-diamminedichloroplatinum(II), *cis*-$[Pt(NH_3)_2Cl_2]$) and related platinum agents are among the most widely prescribed anticancer drugs. The use of cisplatin in medicine traces its origin from the pioneering work of Rosenberg and his intuition that the ability to inhibit the division of bacterial cells could entail the inhibition of cancer cell division.[1] Nowadays, it is well established that the binding of platinum to the N7-position of two adjacent guanosine bases causes unwinding of DNA and disrupts replication, leading to cell death.[2] It is also well documented that platinum complexes may react in the cell with several other biomolecules,[3] leading to altered biological activity. In fact, on the path to their ultimate destination, Pt(II) compounds have a high tendency to bind in particular to N- and S-donor residues in proteins and peptides, which is related to the occurrence of toxic effects.[4] It is therefore important to acquire a detailed knowledge of the cisplatin reactivity with biological ligands because of the possible implications in tuning the response to platinum-based drugs.

The final step of platinum coordination to DNA and the binding to other biomolecules is preceded by aquation processes to form the monoaqua and diaqua species that are believed to be the reactive form of cisplatin and the hydrolysis processes have been studied using a variety of experimental techniques[5] and theoretical approaches.[6] Hydrolysis products of cisplatin, including $[PtCl(NH_3)_2(H_2O)]^+$ and $[Pt(OH)(NH_3)_2(H_2O)]^+$, bear a positive charge and have been identified by mass spectrometry (MS) from electrospray ionization (ESI) of incubated aqueous solutions.[7] The elemental composition has been assigned using Fourier transform ion cyclotron resonance (FT-ICR) mass spectrometry and various MS-based methods have been exploited to analyze DNA-cisplatin adducts.[8] The gas-phase reactivity of platinum complexes with emphasis on bond strengths and CH bond activation is discussed in several reviews.[9]

Aiming to improve the understanding of the mechanism of action of Pt(II) complexes we have undertaken a study of the isolated species in the gas phase, based on IR 'action' spectroscopy and ion-molecule reactivity using mass spectrometry in combination with laser spectroscopy. IR multiple photon dissociation (IRMPD) spectroscopy[10] has revealed distinct vibrational features for *cis*-$[PtCl(NH_3)_2(H_2O)]^+$ and for *trans*-$[PtCl(NH_3)_2(H_2O)]^+$ showing that the two isomers do not interconvert in solution nor in the gas phase under

the sampling conditions.[11] Cisplatin binding to nucleobases and nucleotides has been recently investigated by IRMPD spectroscopy.[12,13] Various simple biomolecules (L) are found to react with cisplatin forming *cis*-$[PtCl(NH_3)_2(L)]^+$ complexes. Structural and reactivity features along the formation path have been examined and form the topic of the present contribution. The selected ligands, including pyridine (Py), 4(5)-methylimidazole (MeIm), thioanisole (TA), and trimethylphosphate (TMP), possess different biomolecular functional groups. The pyridine ring comprises an aza group, functional group present in nucleobases such as adenine and guanine and favored site of cisplatin binding.[12,13] 4(5)-Methylimidazole stands for the heterocyclic substituent of histidine. 4(5)-Methylimidazole exists in a rapidly equilibrating tautomeric mixture of 4-methyl-1H-imidazole and 5-methyl-1H-imidazole (Scheme 1) so there are two possible binding sites for the metal.[14] Thioanisole incorporates the thiomethyl ether group of methionine. The side chain substituents of histidine and methionine are well established binding sites of cisplatin.[15] Trimethylphosphate is chosen to represent the ubiquitous biological phosphates that are also integral part of DNA. Phosphate groups do show affinity for Pt(II) as evidenced both in solution and in gas phase studies.[13,16] The phosphate groups are ionized at physiological pH while trimethylphosphate is neutral but this feature allows it to be used as a reactant in the gas phase. At the same time, it represents an example of 'hard' ligand. Based on the combined information coming from recognition of the charged species by ESI mass spectrometry, kinetic data by gas phase ion-molecule reactivity, structural characterization by IRMPD 'action' spectroscopy and thermodynamic and geometric features from density functional theory (DFT) calculations, reactive events accounting for cisplatin activity are elucidated at the molecular level in a controlled environment with unprecedented detail. The most notable finding lies in the identification of the encounter complex formed by $[PtCl(NH_3)_2(H_2O)]^+$ with the selected ligands, corresponding to the Eigen-Wilkins encounter species for ligand exchange in aqueous solution. This key intermediate is directly detected by ESI for the first time and probed by the IR absorption features.[17]

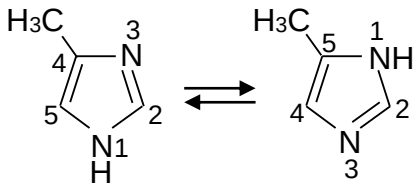

Scheme 1. 4(5)-methylimidazole

Results and discussion

Cisplatin complexes with model ligands: formation of *cis*-$[PtCl(NH_3)_2(L)]^+$ in solution and in the gas-phase

When an incubated aqueous solution of cisplatin is sampled by ESI-MS, the formation of aqua complexes is directly observed (Figure S1(A) in the Supporting Information). Upon mixing with a ligand (L) solution, the *cis*-$[PtCl(NH_3)_2(H_2O)]^+$ aqua complex has largely disappeared while *cis*-$[PtCl(NH_3)_2(L)]^+$ is formed, by substitution of the labile coordinated water molecule. As an example, the mass spectrum reported in Figure S1(B) shows the presence of two prominent species, a cluster centered at m/z 342-344 consistent with the formation of *cis*-$[PtCl(NH_3)_2(Py)]^+$ and a second major species at m/z 360-362 assigned to an adduct corresponding to a $[PtCl(NH_3)_2(Py)(H_2O)]^+$ complex. The isotopic pattern of the two clusters indicates the presence of both one platinum and one chlorine atom, thus confirming the attribution of the observed ions. The formation of the *cis*-$[PtCl(NH_3)_2(L)]^+$ complex is observed also with other tested ligands including TMP, MeIm and TA. It is worth noting that the $[PtCl(NH_3)_2(L)(H_2O)]^+$ cluster, owning formally five ligands, is also present when L is either MeIm or TMP but is not observed for L equal to TA. The ligand substitution reaction occurring in solution has been independently examined in the gas phase [Equation (1)]. The reactant *cis*-$[PtCl(NH_3)_2(H_2O)]^+$ ion, obtained by ESI, has been allowed to react with a neutral L of adequate volatility in the cell of an FT-ICR mass spectrometer and the kinetic progress of the reaction has been recorded.[18] An example of plot showing the time dependence of ion abundances for the reaction with TA is illustrated in Figure S2 in the Supporting Information.

$$cis\text{-}[PtCl(NH_3)_2(H_2O)]^+ + L \rightarrow cis\text{-}[PtCl(NH_3)_2(L)]^+ + H_2O \qquad (1)$$

The reaction efficiency, measuring the % fraction of reactive collisions, varies in the order TMP (2.5) > TA (1.1) > Py (0.41) as shown in Table S1 in the Supporting Information. MeIm was not amenable to the kinetic study because of too low volatility. It is worthy of note that this reactivity trend pertains to the net process involving the naked aqua complex from cisplatin with the selected neutral ligand. Under this condition, the pyridine aza group is found to compete with the thioether function of TA, the reaction efficiencies differing by a factor of less than three, confirming that these two functionalities may compete also in the biological environment. However, in mechanistic studies about platinum anti-tumor drugs at physiological pH, the situation is complicated by the possible incursion of deprotonation of thiol or protonation of N-donor ligands that will markedly affect the reactivity of the biological ligand.[19]

A third route may be envisaged to form *cis*-$[PtCl(NH_3)_2(L)]^+$ in view of the presence of $[PtCl(NH_3)_2(L)(H_2O)]^+$ as abundant species in the ESI mass spectra of the cisplatin/L solutions. When $[PtCl(NH_3)_2(L)(H_2O)]^+$ ions are activated to undergo collision induced dissociation (CID), two fragmentation paths are observed involving either loss of L or loss of water. In the case of Py the branching found at low collision energy is 95/5 [Equation (2)]. When the ligand is MeIm or TMP the branching is 18/82 and 9/91 (Table S2), respectively, and loss of water is largely prevailing.

$$[PtCl(NH_3)_2(Py)(H_2O)]^+ \xrightarrow{CID} \begin{cases} \xrightarrow[5\%]{-H_2O} [PtCl(NH_3)_2(Py)]^+ \\ \xrightarrow[95\%]{-Py} [PtCl(NH_3)(H_2O)]^+ \end{cases}$$

(2)

The question then arises about the structural features of the ligand substitution product *cis*-$[PtCl(NH_3)_2(L)]^+$ obtained from the precursor aqua complex, *cis*-$[PtCl(NH_3)_2(H_2O)]^+$. The latter complex has already been characterized by IRMPD spectroscopy and DFT calculations. In particular, the IR absorptions associated to the NH and OH stretching modes of both *trans*- and *cis*-$[PtCl(NH_3)_2(H_2O]^+$ have been reported in the 3200-3800 cm^{-1} wavenumber range.[11]

Structural features of *cis*-$[PtCl(NH_3)_2(L)]^+$ complexes

The complexes obtained by ligand substitution from *cis*-$[PtCl(NH_3)_2(H_2O)]^+$ have been examined by IRMPD spectroscopy in the mid-IR region,[20] focusing on the species where L is either Py or TMP. When probed by IR multiple photon absorption in resonance with an active vibrational mode, the *cis*-$[PtCl(NH_3)_2(Py)]^+$ complex exhibits sequential losses of NH_3 and HCl. The IRMPD spectrum in the 800-1800 cm^{-1} wavenumber range is plotted in Figure 1. The experimental spectrum is shown together with the computed IR spectrum for the sampled species. The optimized geometry of *cis*-$[PtCl(NH_3)_2(Py)]^+$, also shown in Figure 1 (**Py1**), is characterized by a pyridine plane approximately perpendicular with respect to the square planar coordination at platinum, an eclipsed configuration of the NH_3 ligands and an interaction between chlorine and a hydrogen atom of the adjacent ammonia (Cl···H distance of 2.54 Å). The calculated IR spectrum (upper panel in Figure 1) provides good agreement with the experimental IRMPD spectrum, dominated by a band at 1288 cm^{-1}. This feature comprises the umbrella modes of the two NH_3 ligands expected at 1290 and 1304 cm^{-1}. Weaker bands at 1455 and 1602 cm^{-1} are assigned to CC stretching and asymmetric NH_3 bending modes, as summarized in Table S3 in the Supporting Information reporting the experimental absorbances together with the IR modes calculated for the optimized structure **Py1**.

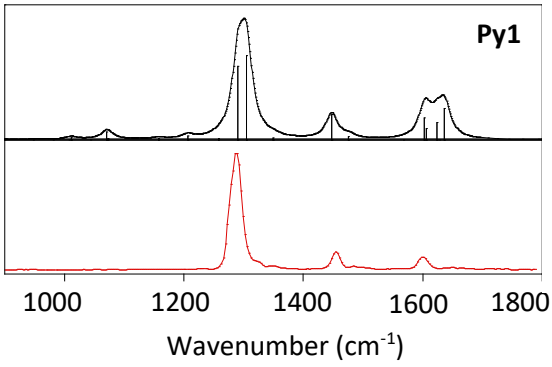

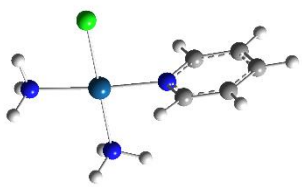

Py1

Figure 1. IRMPD spectrum (lower panel) compared with the IR spectrum of *cis*-$[PtCl(NH_3)_2(Py)]^+$ calculated at B3LYP/6-311+G(d,p) level.

The IRMPD spectrum in the NH stretching range that could add interesting vibrational signatures is not available due to negligible photofragmentation activity under the explored experimental conditions. This finding is not unexpected, though, because of the already scant IRMPD activity of *cis*-$[PtCl(NH_3)_2(H_2O)]^+$, releasing H_2O as fragment.[11] The release of NH_3 observed from *cis*-$[PtCl(NH_3)_2(Py)]^+$ is conceivably more energy demanding and the complex is more resistant to photodissociation.

The TMP complex, *cis*-$[PtCl(NH_3)_2(TMP)]^+$, examined by IRMPD spectroscopy in the mid-IR range, presents major photofragmentation channels involving loss of NH_3 and/or HCl. Figure S3 in the Supporting Information shows the mass spectrum of the isotopic cluster corresponding to *cis*-$[PtCl(NH_3)_2(TMP)]^+$, mass-selected in the FT-ICR cell, together with the mass spectrum following a delay time during which the complex is irradiated at the IR active frequency of 1180 cm^{-1}. Also from this complex, photofragmentation of the intact L ligand is never observed. At variance with the pyridine ligand, TMP presents two potential sites for platinum binding and calculations have been performed taking into account the possible formation of two distinct isomers. In the first one (**TMP1**) shown in Figure 2, Pt is coordinated to the phosphoryl oxygen while in the second one (**TMP2**) Pt is bound to a methoxyl oxygen. Vibrational analysis of the optimized structures **TMP1** and **TMP2** yields the calculated IR spectra plotted in the upper panels of Figure 2. The first isomer **TMP1** is more stable by 43 kJ mol^{-1} (thermodynamic data can be found in Table S4 in the Supporting Information) and the calculated IR spectrum of **TMP1** is consistent with the observed IRMPD features, showing the phosphoryl group to be the coordination site. Experimental bands and calculated IR resonances of **TMP1** are listed in Table S3 in the Supporting Information. The IRMPD spectrum of *cis*-$[PtCl(NH_3)_2(TMP)]^+$ is characterized by two prominent bands at 1071 and 1178 cm^{-1}, assigned to P-OCH_3 and P-OPt stretching modes, respectively. One may compare the free phosphoryl stretching mode of **TMP2** at 1280 cm^{-1} with the P-OPt stretching in **TMP1** calculated at 1152 cm^{-1}. The observed decrease in the calculated frequencies goes in parallel with the lengthening of the P-O bond from 1.480 Å in **TMP2** to 1.520 Å in **TMP1**, an effect of the coordination with platinum, reducing the P=O bond strength. The broad IRMPD band at 1071 cm^{-1} is assigned to a convolution of three P-OCH_3 stretches with similar frequencies, at 1066, 1074 and 1086 cm^{-1}. In contrast, a distinct IR signature of **TMP2** at 943 cm^{-1}, associated to the P-O stretch involving the methoxyl group coordinated to platinum, is missing in the experimental spectrum. The umbrella modes of the two NH_3 ligands calculated at 1286 and 1317 cm^{-1} for **TMP1** account for the weak experimental signatures at 1271 and 1295 cm^{-1}. Other tested isomers have included **TMP3**, a conformer of **TMP1** displaying a methoxyl group oriented towards the neighbouring ammonia to allow a NH···OCH_3

hydrogen bond interaction. This species, lying at 9.4 kJ mol^{-1} relative to **TMP1**, shows an IR spectrum in poor agreement with the experiment (Figure S4 in the Supporting Information), in particular owing to a red-shifted P-OCH_3 stretching frequency of the group involved in hydrogen bonding with ammonia (at 1051 cm^{-1}). Also depicted in Figure S4 is the optimized structure and calculated IR spectrum of the *trans*-$[PtCl(NH_3)_2(TMP)]^+$ isomer **TMP4**, rather disproving its presence in the sampled ion population.

Thus, for both complexes *cis*-$[PtCl(NH_3)_2(L)]^+$, where L is either Py or TMP, the experimental IRMPD spectra are well interpreted by the IR spectra of the optimized geometry of the most stable isomer. The coordinates of the optimized geometries of *cis*-$[PtCl(NH_3)_2(L)]^+$ complexes are collected in Table S-A in the Supporting Information. Additionally, the IRMPD spectrum of the $[PtCl(NH_3)_2(MeIm)]^+$ has also been recorded. However, this species is poorly active and just one band at 1294 cm^{-1} is observed. The spectrum is shown in Figure S5 together with the calculated IR spectra for the two potential isomers differing for the position of the methyl group. Both calculated spectra can account for the IRMPD feature at 1294 cm^{-1} while other predicted bands of lower intensity (less than 50 km mol^{-1}) are missing in the experimental spectrum. This finding is not unexpected though, based on previous reports showing that modes of low activity for species presenting high dissociation thresholds may fail to be observed.[10b,21]

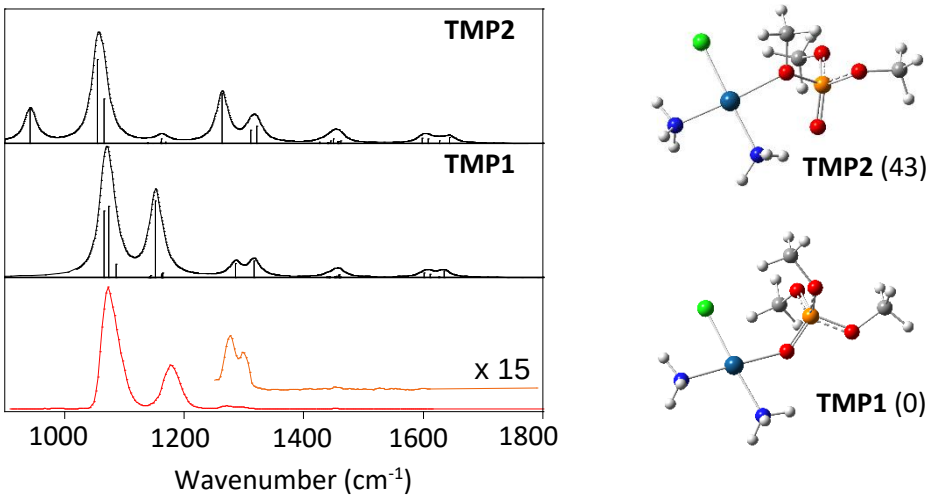

Figure 2. IRMPD spectrum (red) compared with the IR spectra of *cis*-$[PtCl(NH_3)_2(TMP)]^+$ calculated at B3LYP/6-311+G(d,p) level. Relative energies (in kJ mol^{-1} at 298K) of optimized structures are obtained at ωB97X-D/6-311+G(d,p) level.

Cisplatin-derived complexes with five nominal ligands: $[PtCl(NH_3)_2(L)(H_2O)]^+$

Complexes of platinum(II) presenting a total of five potential ligands, $[PtCl(NH_3)_2(L)(H_2O)]^+$, are obtained by ESI as abundant ionic species when L is equal to Py, MeIm and TMP. Any structural assignment should account for their fragmentation behavior when sampled by CID, involving loss of either L or H_2O. In order to elucidate this conduct, different hypotheses about the structure of the isolated ions can be conceived and several possible isomers of $[PtCl(NH_3)_2(L)(H_2O)]^+$ ions have been investigated by DFT using either the

B3LYP hybrid functional, that is known to perform well in yielding IR spectra and is uniformly adopted to provide comparison with IRMPD spectra, or ωB97X-D, which includes empirical dispersion and is referred to for relative energy considerations. Five-coordinate Pt(II) complexes are not commonly observed in the gas phase by mass spectrometry though evidence has been reported from x-ray structural analysis.[22] More likely, the structure of the $[PtCl(NH_3)_2(L)(H_2O)]^+$ complex is accounted for by a square planar, four-coordinate Pt(II) complex interacting with an additional molecule, either L or H_2O, weakly bound in an 'external' coordination level. Indeed, in the association of hydrogen bond donors, such as H_2O, with platinum(II) complexes, a role has been ascribed to both HO-H···Pt and H_2O···Pt interactions[23] and experimental evidence for Pt···H hydrogen bonding interactions both in solution and in the solid state have been reported.[23e] Accordingly, a computational survey of potential structures for $[PtCl(NH_3)_2(L)(H_2O)]^+$ complexes has included various starting geometries with an axial approach of a water molecule to a square planar $[PtCl(NH_3)_2(L)]^+$ complex. However, on geometry optimization of all sampled complexes (L = Py, MeIm, and TMP) the water molecule ended in an 'external' solvating interaction with the square planar *cis*-$[PtCl(NH_3)_2(L)]^+$ complex, as shown by the isomeric structures depicted in Figure 3. A complete overview of all sampled structures is presented in Figure S6 and the coordinates of optimized geometries are listed in Table S-B in the Supporting Information. For example, when the ligand is pyridine, the solvating water molecule may either interact with the positively polarized hydrogen atoms of the two NH_3 ligands (isomer **Py_1**) or establish a bridging interaction with an ammonia proton on one side and the chlorine atom on the other (isomer **Py_2**), the former isomer being energetically favored by 10 kJ mol^{-1}. However, a third isomer may be envisioned for $[PtCl(NH_3)_2(L)(H_2O)]^+$, involving the added ligand L 'externally' bound to the aqua complex (isomer **Py_3**). The ensuing species corresponds to the encounter complex of the incoming ligand with the reactant *cis*-$[PtCl(NH_3)_2(H_2O)]^+$. The aza group of pyridine is basic enough that in interacting with the polarized hydrogen of the aqua ligand a proton transfer event is occurring. The presence of **Py_3** is suggested by the prevailing loss of Py from $[PtCl(NH_3)_2(L)(H_2O)]^+$ upon CID activation. However, precise evidence on the structure of the sampled complexes can be obtained by IRMPD spectroscopy, as described in the following paragraph.

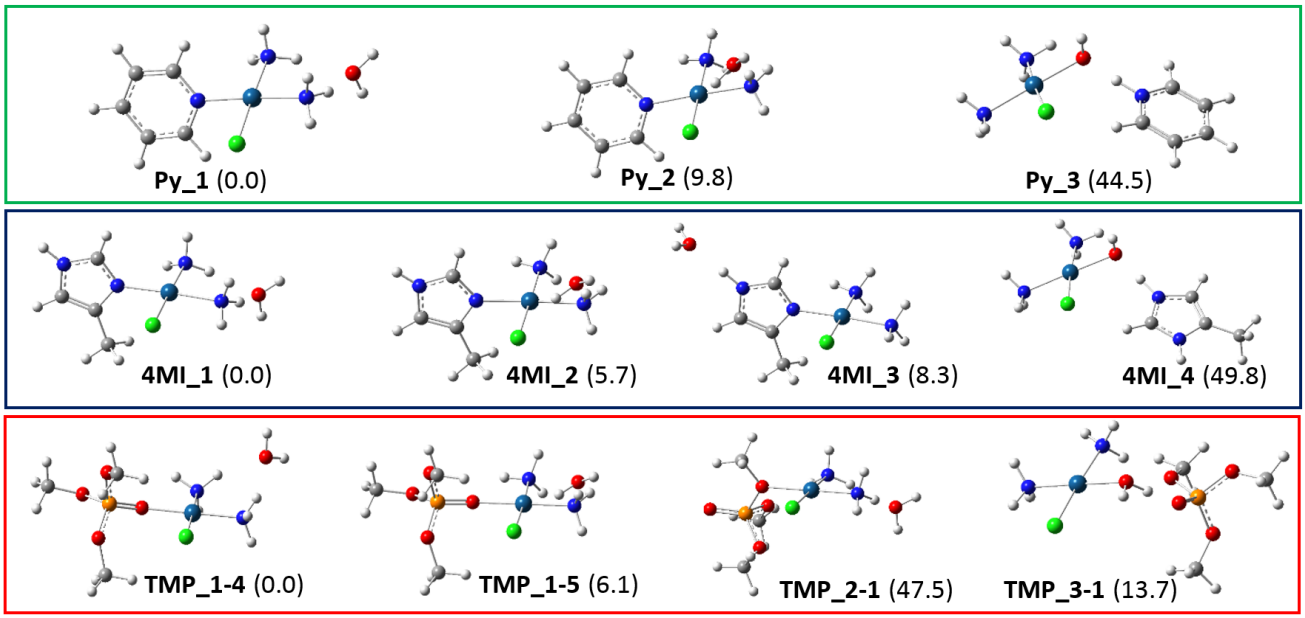

Figure 3. Structures of $[PtCl(NH_3)_2(L)(H_2O)]^+$ complexes optimized at B3LYP/6-311+G(d,p) (LanL2TZ for Pt) level of theory.

The aza group of pyridine is the unique site in the molecule available for platinum or proton binding. The other tested ligands present a more complex binding pattern, owning multiple reactive sites. MeIm presents two non-equivalent aza groups differing for the position of the methyl group, due to the tautomeric equilibrium. Furthermore, the NH group in the imidazole ring may act as hydrogen bond donor towards a solvating water molecule. Thus, three different structures may represent the $[PtCl(NH_3)_2(L)(H_2O)]^+$ complex with the metal coordinated to 4-methylimidazole and a solvating water molecule, **4MI_1**, **4MI_2**, and **4MI_3**. Alternatively, 4-methylimidazole can be 'externally' bound with the aqua complex *cis*-$[PtCl(NH_3)_2(H_2O)]^+$, yielding complex **4MI_4**, and the interaction is governed by a strong bond mediated by the hydrogen on the water ligand and 4-methylimidazole. Indeed, within the complex the proton appears to reside on the nitrogen atom rather than on oxygen, though upon CID the product ion is *cis*-$[PtCl(NH_3)_2(H_2O)]^+$ and neutral MeIm is released. In agreement with the CID results, the proton affinity (PA) of *cis*-$[PtCl(NH_3)_2(OH)]$ is calculated equal to 964 kJ mol^{-1}, higher than the 953 kJ mol^{-1} value for MeIm,[24] the most basic among the selected ligands. However, the ion-neutral binding energy favors the formation of the {*cis*-$[PtCl(NH_3)_2(OH)]$ $(MeImH)^+$} pair relative to {*cis*-$[PtCl(NH_3)_2(H_2O)]^+$ (MeIm)}, so counterbalancing the relative PA values that refer to the isolated species. A comparable set of complexes, **5MI_1** to **5MI_4**, entail binding of the 5-methylimidazole tautomer and are depicted in Figure S6. The difference between the two sets lies in the position of the methyl group which is found not to affect to any relevant extent the relative energies nor, as underlined in the following paragraph, the vibrational properties in each pair of corresponding structures. For example, **5MI_2** is only 2 kJ mol^{-1} higher in energy relative to **4MI_2**.

When the ligand is TMP the collection of possible structures for $[PtCl(NH_3)_2(L)(H_2O)]^+$ becomes increasingly populated because of the two sites available for coordination, phosphoryl- and methoxyl-oxygen, and of the higher conformational flexibility. A few stable structures are shown in Figure 3 and the complete series is presented in Figure S6. Isomer **TMP_1-4** is the most stable in the **TMP_1-n** series of structures, characterized by phosphoryl platination and solvation by water. The interaction of water with both NH_3 ligands, as present in **TMP_1-4**, is confirmed to be favored with respect to other solvating motifs. This finding is also confirmed by the most stable member, **TMP_2-1**, in the **TMP_2-n** series, characterized by platination at the methoxyl oxygen. Finally a third family of conformers is obtained for the *cis*-$[PtCl(NH_3)_2(H_2O)]^+$ complex solvated by TMP. The most stable one is **TMP_3-1**, presenting the phosphoryl-oxygen engaged in hydrogen bonding with a highly polarized hydrogen on the aqua ligand and a methoxyl oxygen interacting with the adjacent NH_3. In the next three isomers, **TMP_3-2**, **TMP_3-3**, and **TMP_3-4**, TMP is placed in a bridging position between H_2O/Cl, H_2O/NH_3, and NH_3/NH_3 ligands, respectively.

Interestingly, while the relative energies of **TMP_3-n** isomers are very close based on the B3LYP functional, inclusion of dispersion effects with the ωB97X-D functional renders **TMP_3-1** considerably more stable than the other isomers. The computed thermodynamic data for all cited clusters are reported in Table S4 in the Supporting Information.

IR spectroscopy of $[PtCl(NH_3)_2(L)(H_2O)]^+$ cluster ions

In order to gain insight into the structure of the complexes responding to $[PtCl(NH_3)_2(L)(H_2O)]^+$ composition, IRMPD spectroscopy has been performed in two spectral ranges, 900-1900 and 2900-3700 cm^{-1}.[20,25] At variance with *cis*-$[PtCl(NH_3)_2(L)]^+$ complexes, $[PtCl(NH_3)_2(L)(H_2O)]^+$ ions are highly active in IRMPD, in agreement with the theoretical results predicting the structure of a four-coordinate complex associated with a solvating molecule. These clusters are in fact expected to be more prone to photofragmentation than the covalently bound *cis*-$[PtCl(NH_3)_2(L)]^+$ complexes.

The IRMPD process of selected $[PtCl(NH_3)_2(L)(H_2O)]^+$ complexes (L = Py, MeIm, and TMP) leads to two products, either *cis*-$[PtCl(NH_3)_2(H_2O)]^+$ or *cis*-$[PtCl(NH_3)_2(L)]^+$, namely the same products of ligand and water loss that were observed upon CID. Also the branching ratio for L/H_2O loss is similar, corresponding to 86/14, 19/81, and 2/98 in the case of L equal to Py, MeIm, and TMP, respectively (Table S2). Incidentally, the *cis*-geometry has been probed in the *cis*-$[PtCl(NH_3)_2(H_2O)]^+$ fragment obtained by CID of $[PtCl(NH_3)_2(Py)(H_2O)]^+$. The ion, assayed by IRMPD spectroscopy, displays an absorption pattern (Figure S7) consistent the *cis*-aqua complex that has already been described.[11] In view of the computational survey, the $[PtCl(NH_3)_2(L)(H_2O)]^+$ cluster is expected to conform to a four-coordinate platinum(II) complex solvated by either L or H_2O. The appearance of two dissociation routes may suggest the presence of two distinct families of cluster ions, namely *cis*-$[PtCl(NH_3)_2(L)](H_2O)^+$ and *cis*-$[PtCl(NH_3)_2(H_2O)](L)^+$, with a solvating water or ligand molecule, respectively. However, the comparable profile for L and H_2O loss channels in the IRMPD spectra of $[PtCl(NH_3)_2(L)(H_2O)]^+$ ions speaks against this notion, supporting rather a single species undergoing competing fragmentation paths (see Figure S8 in the Supporting Information). Therefore, an analysis of the IRMPD vibrational signatures is fundamental for an understanding of the structure of the clusters.

Figure 4 shows the IRMPD spectrum of $[PtCl(NH_3)_2(Py)(H_2O)]^+$ together with the IR spectra calculated for **Py_1** and **Py_3**. The IR spectrum of **Py_3** is clearly the one matching the experiment while the IR spectrum of **Py_1** and also the one of **Py_2** (reported in Figure S9 in the Supporting Information) present considerable discrepancy. The experimental bands and the assigned vibrational modes of **Py_3** are listed in Table S5 in the Supporting Information. However, few significant features may be mentioned. The broad IRMPD absorbance at 955 cm^{-1} is associated with the IR modes at 932-983 cm^{-1} due to OH bends of the aqua ligand. The two strong IRMPD signals at 1259 and 1292 cm^{-1} are related to the NH_3 umbrella modes that are conserved in all structures, though their separation is well matched only in the IR spectrum of **Py_3** (35 cm^{-1}). In the OH stretch range, the symmetric and asymmetric stretching modes of the solvating water at 3625

and 3708 cm^{-1} in the IR spectrum of **Py_1** are missing in the IRMPD spectrum whereas the OH stretch of the hydroxo ligand of **Py_3** at 3640 cm^{-1} accounts for the only one experimental feature in this range, at 3610 cm^{-1}.

A weak signature at 3094 cm^{-1} in the IRMPD spectrum has a counterpart in the IR spectrum of **Py_3** at 3054-3058 cm^{-1}. This feature, characteristic of **Py_3**, is associated to the CH stretch of the bond directed towards the chlorine atom. The assignment has been probed using perdeuterated pyridine as ligand. In the ensuing IRMPD spectrum the band at 3094 cm^{-1} has vanished (the expected red shift at 2264 cm^{-1} moves this absorption outside the experimental range) while the signal at 3296 cm^{-1}, due to symmetric stretches of NH_3, has remained approximately unchanged (see Figure S10 in the Supporting Information).

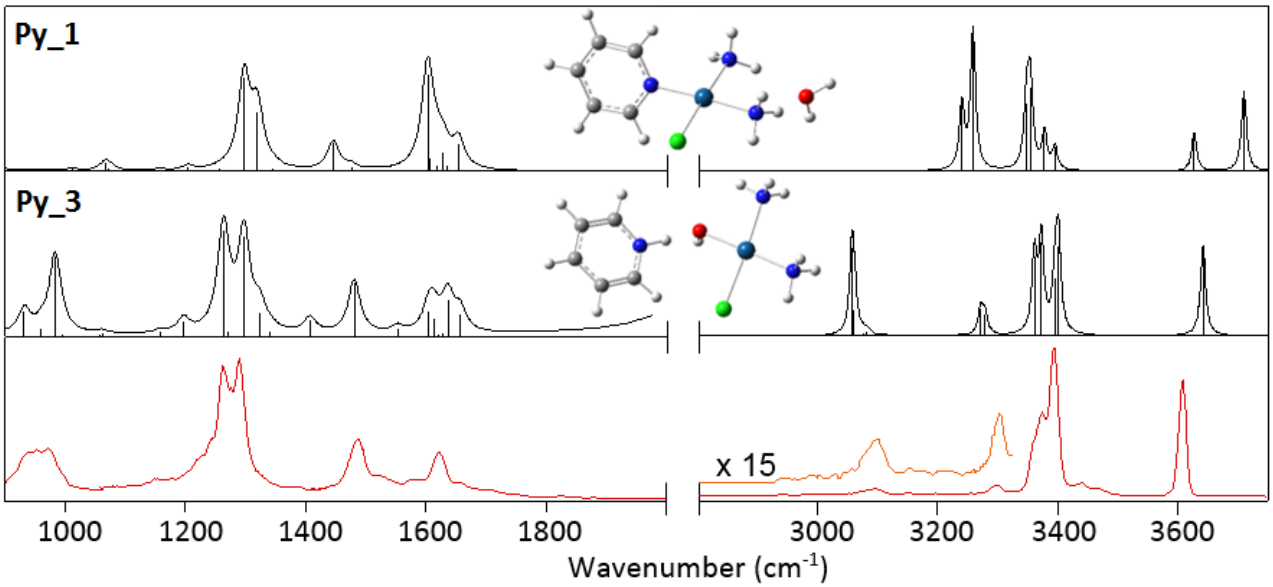

Figure 4. IRMPD spectrum (in red) of $[PtCl(NH_3)_2(Py)(H_2O)]^+$ and calculated IR spectra of **Py_1** and **Py_3**.

Therefore the IRMPD assay of $[PtCl(NH_3)_2(Py)(H_2O)]^+$ is consistent with an addition complex of pyridine with the primary hydrolytic product of cisplatin. This finding explains the loss of pyridine from the complex but at the same time it implies that a rearrangement is occurring to allow the competing loss of water and formation of the substitution complex.

$[PtCl(NH_3)_2(MeIm)(H_2O)]^+$ complexes sampled by IRMPD spectroscopy present similar features as discerned for $[PtCl(NH_3)_2(Py)(H_2O)]^+$ ions (Figure 5). In the most informative region, 2900-3800 cm^{-1}, the IRMPD spectrum is remarkably well fitted by the IR spectrum pertaining to an isomer such as **4MI_4**, holding an externally bound MeIm. Once again, the pattern of the symmetric and asymmetric H_2O stretches,

that characterizes a solvating water molecule as in **4MI_1**, is not observed experimentally. In this case, the fingerprint region is less diagnostic, although the prominent maxima at 1259 and 1289 cm^{-1} are well accounted for by the NH_3 umbrella modes calculated at 1262 and 1294 cm^{-1} in the IR spectrum of **4MI_4** (Table S6 in the Supporting Information). The resonance at 1206 cm^{-1} ascribed to an in plane CH bend of imidazole in **4MI_4** also explains the shoulder on the red side of this prominent band. The unresolved signature with maxima at 1083 and 1133 cm^{-1} is not explained by the IR spectrum of isomer **4MI_4** alone but is consistent with a contribution of isomer **5MI_4** (Table S6 and Figure S11 in the Supporting Information). Cluster isomers differing for the position of the methyl group, as in the **4MI_n** and **5MI_n** series, are very close in energy and also the IR spectra are quite similar, only differing for minor features as shown in Figure S11.

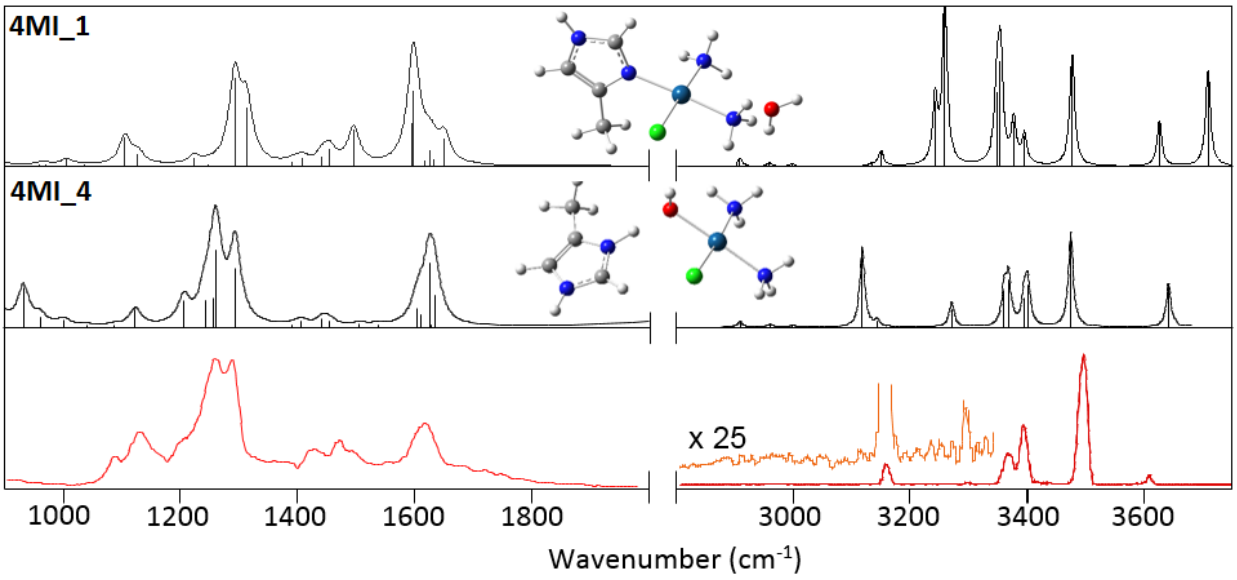

Figure 5. IRMPD spectrum (in red) of $[PtCl(NH_3)_2(MeIm)(H_2O)]^+$ and calculated IR spectra of **4MI_4** and **4MI_1**.

In the higher frequency range, a band at 3160 cm^{-1} is consistent with the CH stretch of the imidazole hydrogen oriented towards chlorine. This signal has a counterpart in the one at 3094 cm^{-1} reported in the IRMPD spectrum of $[PtCl(NH_3)_2(Py)(H_2O)]^+$. The weak band at 3294 cm^{-1} is ascribed to the NH_3 symmetric stretch, while the two bands at 3359 and 3393 cm^{-1} are associated to the NH_3 asymmetric stretch. The most important absorption of this region is the NH stretch of imidazole at 3497 cm^{-1} that is conserved in all computed spectra except the ones of clusters characterized by a solvating water bound to the imidazole NH. In this latter case, the NH stretch presents a significant red shift.

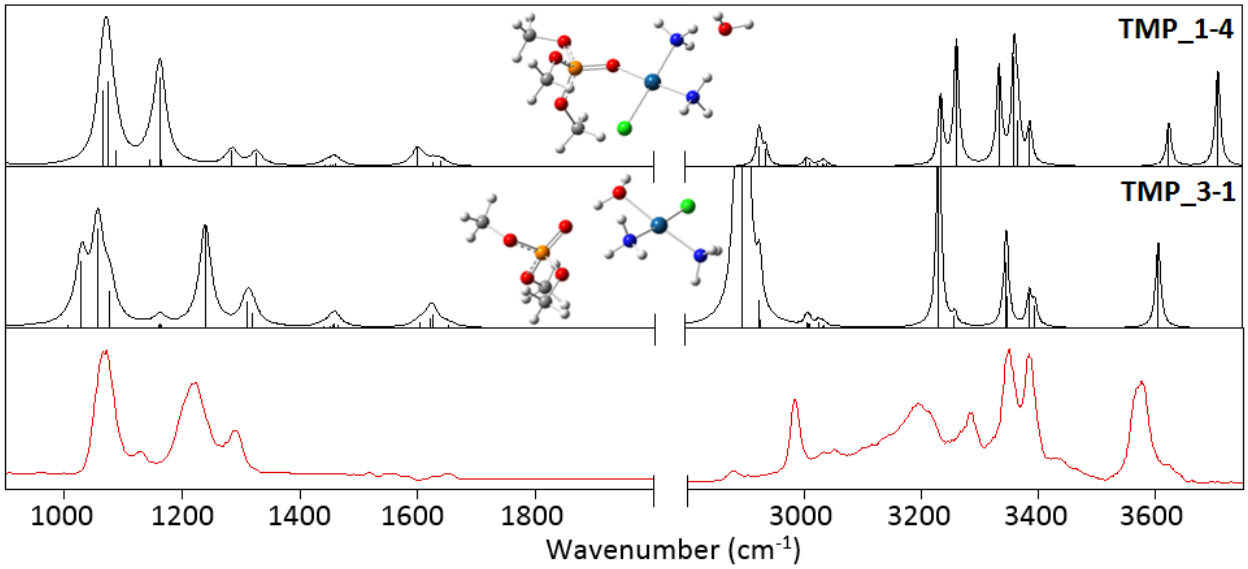

Figure 6. IRMPD spectrum (in red) of $[PtCl(NH_3)_2(TMP)(H_2O)]^+$ and calculated IR spectra of **TMP_1-4** and **TMP_3-1**.

The IRMPD assay of $[PtCl(NH_3)_2(TMP)(H_2O)]^+$ clusters reveals that also in this case the sampled species conforms to a four coordinate *cis*-$[PtCl(NH_3)_2(H_2O)]^+$ aqua complex solvated by the added ligand. This finding is clearly shown in Figure 6 (and Table S7) where the IRMPD spectrum is compared with the IR spectra of **TMP_1-4** and **TMP_3-1**, exemplifying isomers with solvating water and solvating TMP, respectively. With respect to Py and MeIm ligands, TMP is endowed with greater conformational freedom so that the number of conformers to be taken into account within each class of isomers is considerably large. This fact explains the large bandwidth of several features in the IRMPD spectrum, testifying the presence of multiple species of similar energy. In the following discussion the focus is on the prototypical isomers **TMP_1-4** and **TMP_3-1**. Inspecting Figure 6, direct coordination of TMP to Pt(II) may be discarded in view of the missing feature at 1162 cm^{-1}, highly active in the IR spectrum of isomer **TMP_1-4**. The associated vibrational mode, the P-O stretch of the formerly phosphoryl double bond, is remarkably red-shifted as a consequence of coordination to the metal. The frequency is in fact 1239 cm^{-1} in the spectrum of **TMP_3-1**, accounting for the prominent IRMPD band 1220 cm^{-1}. This motif appears then to discriminate between alternative molecular structures. In contrast, the P-OCH_3 stretches, responsible for the band at 1068 cm^{-1}, are conserved in all isomers. The band at 1286 cm^{-1} is due to symmetric NH_3 bending (umbrella) modes. The band at highest frequency is the OH stretch at 3573 cm^{-1}. The rather large width and the presence of a shoulder on the blue side are evidence for the contribution of multiple conformers (e.g. **TMP_3-1** and **TMP_3-2**, see Figure S12). As in the case of the Py and MeIm complexes, the absence of the asymmetric

OH stretch of water at ca. 3700 cm^{-1} allows to discard any contribution of a water solvated cluster such as **TMP_1-4**. The two bands at 3346 and 3380 cm^{-1}, the asymmetric NH stretches of NH_3 ligands, are a common pattern in the IRMPD spectra of all sampled $[PtCl(NH_3)_2(TMP)(H_2O)]^+$ clusters. The absorption at 3280 cm^{-1} is assigned to the symmetric stretches of ammonia while the broad signal at 3200 cm^{-1} is consistent with the stretching mode of the NH bond involved in hydrogen bonding with a TMP methoxyl group.

To summarize, all sampled $[PtCl(NH_3)_2(L)(H_2O)]^+$ clusters assayed by IRMPD spectroscopy reveal the nature of *cis*-$[PtCl(NH_3)_2(H_2O)]^+$ complex solvated by the L molecule. The ligand is typically hydrogen bonded to the aqua ligand and, when L is basic enough as in the case of Py and MeIm, the proton may rather reside on the L partner within the complex.

Ligand substitution in the encounter complex of L and *cis*-$[PtCl(NH_3)_2(H_2O)]^+$

The combined information from the reactivity pattern, the computational survey and the IRMPD analysis of ESI formed $[PtCl(NH_3)_2(L)(H_2O)]^+$ ions has revealed the dynamics of a well characterized cluster corresponding to the encounter complex of a ligand with *cis*-$[PtCl(NH_3)_2(H_2O)]^+$, namely the primary hydrolytic product of cisplatin. The $[PtCl(NH_3)_2(L)(H_2O)]^+$ ions, holding Pt(II) and five potential ligands, formed in an aqueous solution of cisplatin and ligand L, has in fact revealed the structure of a cluster of L associated with *cis*-$[PtCl(NH_3)_2(H_2O)]^+$. When the cluster is imparted excess energy, either by non-reactive collisions or by multiple IR photon absorption, thus activated to undergo dissociation, in a considerable fraction of events water is released. Loss of the 'external' ligand would be the expected, entropy driven dissociation path. Loss of water implies that in the activated cluster a net ligand exchange process is taking place within the isolated reactant pair. When the process occurs under IRMPD conditions, it is reminiscent of the infrared induced reactivity of nitrogen oxides on rhodium clusters that has revealed elementary steps in a catalytic reaction,[26] showing that IRMPD spectroscopy can provide information about the structure of the metal cluster, the state of the absorbed molecules and the degree of bond activation.

Mechanistic insight into the bimolecular, CID-activated and IR-induced reactivity behavior has been sought from a survey of the potential energy surface (PES) connecting the conceivable species. Thermodynamic data are collected in Table S4. A schematic of the PES is shown in Figure 7. Relative enthalpies at 298K are reported at both B3LYP/6-311+G(d,p) and ωB97X-D/6-311+G(d,p) level of theory (LanL2TZ for Pt). The following discussion is based on ωB97X-D/6-311+G(d,p) data. Relative enthalpies are referred to the most stable isomer for the *cis*-$[PtCl(NH_3)_2(H_2O)](L)^+$ cluster with the 'external' ligand, namely **4MI_4** (L = MeIm), **Py_3** (L = Py), **TMP_3-1** (L = TMP), and **TA_2** (L = TA). The energy released with respect to the separated *cis*-$[PtCl(NH_3)_2(H_2O)]^+$ + L pair is comprised between 138 and 159 kJ mol^{-1} for Py, TMP and MeIm. In the case of TA the binding energy is markedly lower, 88 kJ mol^{-1}, which likely accounts for the failure to obtain *cis*-$[PtCl(NH_3)_2(H_2O)](TA)^+$ clusters by ESI.

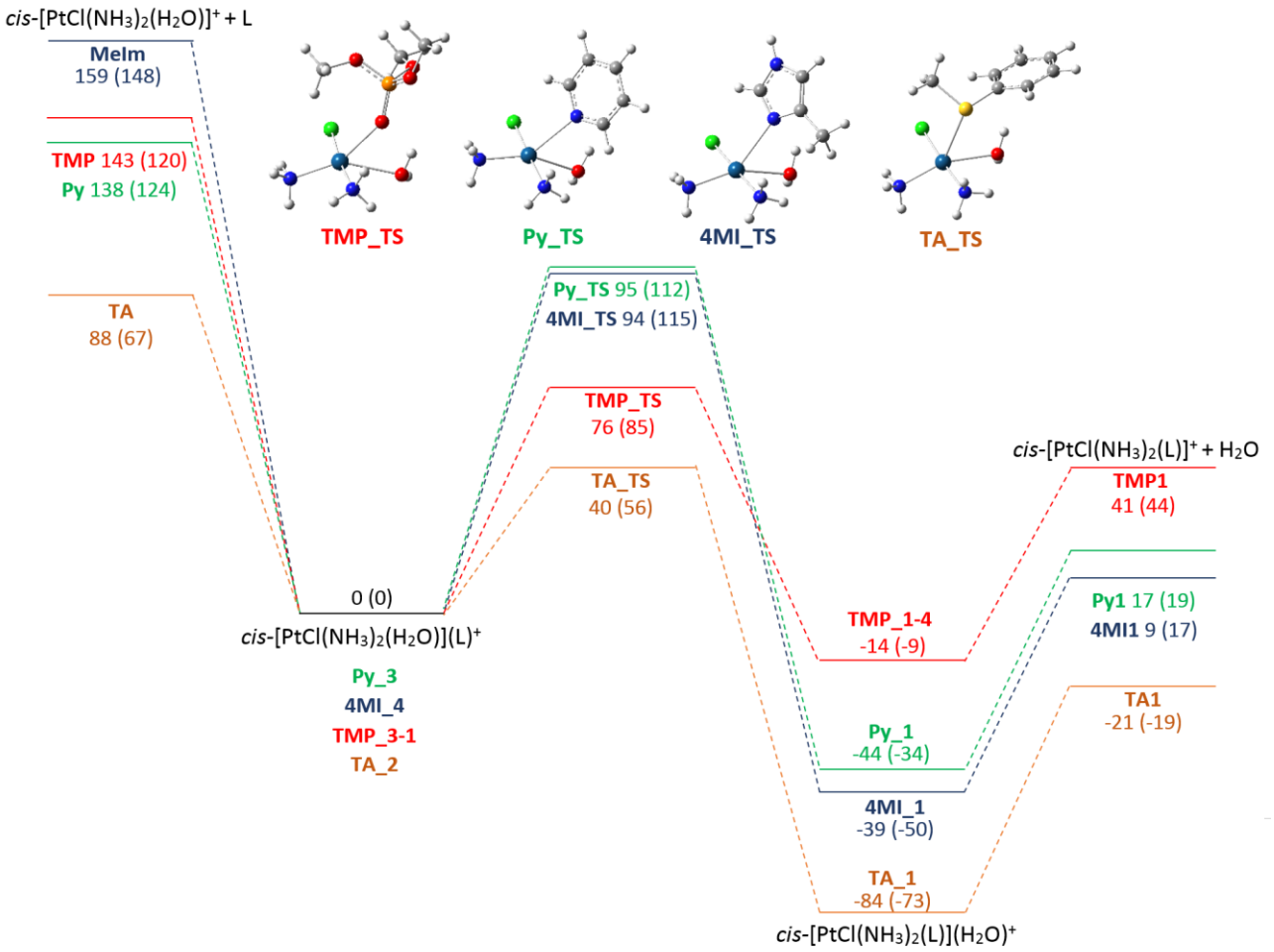

Figure 7. PES for the reaction of *cis*-$[PtCl(NH_3)_2(H_2O)]^+$ with L (L= Py, 4-MeIm, TMP, TA). Geometries of the transition states computed at B3LYP/6-311+G(d,p) level are shown. Relative enthalpies (kJ mol^{-1}) are reported as obtained at ωB97X-D/6-311+G(d,p) (values at B3LYP/6-311+G(d,p) level are in brackets).

The *cis*-$[PtCl(NH_3)_2(H_2O)](L)^+$ complex may rearrange to *cis*-$[PtCl(NH_3)_2(L)](H_2O)^+$ by way of a transition state involving pentacoordination at Pt(II). The structures of the transition states are depicted in Figure 7 while the structures of all stable species appearing in Figure 7 are reported in Figure S6 and their coordinates are provided in Tables S-A and S-B.

Ligand exchange within the *cis*-$[PtCl(NH_3)_2(H_2O)](L)^+$ cluster is exothermic in all cases. The reaction of TA is the most strongly favored ($\Delta H° = -84$ kJ mol^{-1}) and is also characterized by the lowest activation barrier

(40 kJ mol^{-1}). The binding of Pt(II) with the sulfur ligand is so favored that even the dissociation into products, *cis*-$[PtCl(NH_3)_2(TA)]^+ + H_2O$, is still exothermic, again in line with the lack of any observed *cis*-$[PtCl(NH_3)_2(H_2O)](TA)^+$ clusters. The bimolecular reactivity of TA with *cis*-$[PtCl(NH_3)_2(H_2O)]^+$ is not the highest, though, as determined in the FT-ICR cell. Here, the single collision regime at the prevailing low pressure points to the difference between the back dissociation energy of the *cis*-$[PtCl(NH_3)_2(H_2O)](L)^+$ collision complex and the activation energy for ligand exchange as the key parameter determining relative efficiencies.[27] This difference is equal to 67, 48, and 43 kJ mol^{-1} in agreement with the % reaction efficiencies of 2.5, 1.1, and 0.41 for the tested series of ligands, TMP, TA, and Py, respectively, in the bimolecular ligand substitution [Equation (1)]. The PES outlined in Figure 7 in fact conforms to Brauman's 'double well' potential energy surface model that explains the kinetic behavior of ion-molecule reactions at low pressure, in the absence of collisions with a bath gas.[27] Even if the central barrier is lower than the energy of the separated reactants, it can be more likely for the collision complex (*cis*-$[PtCl(NH_3)_2(H_2O)](L)^+$ in Figure 7) to dissociate back to the free reactants because this process is entropically more favorable. As a consequence, the rate of the reaction may not reach the collision controlled limit and in the present case the observed reaction efficiencies are well below 100%. Taking into account the common entropic bias towards back dissociation, the difference in energy between separated (*cis*-$[PtCl(NH_3)_2(H_2O)]^+$ + L and the transition state for ligand exchange will govern the branching into the two channels.[27] The same energy difference is expected to control the branching of isolated *cis*-$[PtCl(NH_3)_2(H_2O)](L)^+$ clusters when activated to fragment by L or H_2O loss. Indeed, the calculated energy differences of 67, 65, and 43 kJ mol^{-1} for TMP, MeIm, and Py clusters, respectively, is in line with the decreasing fraction of H_2O loss along the series. In other words, all *cis*-$[PtCl(NH_3)_2(H_2O)](L)^+$ clusters face competition between two channels both involving considerable energy barriers. Dissociation of 'externally' bound L is consistently more endothermic but is entropically favored. Ligand substitution to yield *cis*-$[PtCl(NH_3)_2(L)](H_2O)^+$ is a process proceeding by a tight transition state, highly organized and with relatively wide separation between internal energy levels. So, statistically, there will be a smaller number of accessible states available at a given energy for the system to progress through the central barrier.[27] Thus, the calculated PES provides a congruent rationale for the observed reactivity pattern.

The PES also provides a motivation for observing *cis*-$[PtCl(NH_3)_2(H_2O)](L)^+$ clusters from the ESI process rather than the more stable *cis*-$[PtCl(NH_3)_2(L)](H_2O)^+$ isomers. As stated above, the binding energy of *cis*-$[PtCl(NH_3)_2(H_2O)](TA)^+$ of 88 kJ mol^{-1} is apparently too low to deliver this species by ESI. According to the PES data, the water binding energy in *cis*-$[PtCl(NH_3)_2(L)](H_2O)^+$ complexes (L = MeIm, TMP, TA, Py) is ≤ 63 kJ mol^{-1}, well below 88 kJ mol^{-1}, thus hampering their sampling under the prevailing experimental conditions. Alternative means to isolate these clusters will be the topic of forthcoming efforts.

Conclusions

The primary hydrolytic product of cisplatin, *cis*-$[PtCl(NH_3)_2(H_2O)]^+$, is exposed to reaction with several biological ligands both in solution and in the gas phase and the ligand exchange process with representative functional groups has been investigated at the molecular level in an isolated environment. The encounter complex of the ligand L with *cis*-$[PtCl(NH_3)_2(H_2O)]^+$, formed in solution, evolves into the *cis*-$[PtCl(NH_3)_2(L]^+$ substitution product, delivered into the gas phase and assayed by IRMPD spectroscopy. Structural features of *cis*-$[PtCl(NH_3)_2(L]^+$ have thus been unveiled for Py, TMP, and, in lesser detail, MeIm. The structural analysis is based on the experimental IRMPD spectra which are examined in conjunction with the IR spectra from a thorough computational survey of potential candidates. The $[PtCl(NH_3)_2(L)(H_2O)]^+$ complex is found to conform to the aqua complex *cis*-$[PtCl(NH_3)_2(H_2O)]^+$ interacting with an externally bound L molecule, namely the encounter complex formed in solution along the path of the ligand exchange process. Thus, the *cis*-[$[PtCl(NH_3)_2(H_2O)]$ $(L)^+$ cluster is a prototypical example of the encounter complex in the Eigen-Wilkins reactant preassociation model of ligand interchange in metal complexes in aqueous solution. In this framework, the substitution by an incoming ligand into the first coordination sphere is always preceded by its entry into the second coordination sphere. The stepwise process is synthetically depicted as

$M^{m+} + L^{x-} \rightleftarrows M\cdot(OH_2)\cdot L^{(m-x)+} \rightleftarrows ML^{(m-x)+}$ where $M\cdot(OH_2)\cdot L^{(m-x)+}$ represents the aqua complex of M^{m+} associated to L^{x-} in the outer coordination sphere, corresponding to the 'external' interaction of L within *cis*-$[PtCl(NH_3)_2(H_2O)]$ $(L)^+$. These adducts are assigned a key role in the initial steps involved in the substitution mechanisms of cisplatin[6g,i] and related antitumoral molecules.[28] This inference from theoretical studies of cisplatin activation both in the gas phase and in solution is now supported by the experimental evidence presently obtained. The $[PtCl(NH_3)_2(H_2O)](L)^+$ cluster does in fact yield *cis*-$[PtCl(NH_3)_2(L)]^+$, by ligand substitution followed by loss of H_2O, when it is activated by energetic collisions or in the same IR multiple photon absorption process that is exploited to reveal the vibrational features in IRMPD 'action' spectroscopy. The branching of the $[PtCl(NH_3)_2(H_2O)](L)^+$ cluster into dissociation by either L or H_2O loss is directed by the balance between the L dissociation energy and the activation barrier for water ligand substitution. The same energy difference is responsible for the bimolecular reactivity observed in the *cis*-$[PtCl(NH_3)_2(H_2O)]^+ + L \rightarrow$ *cis*-$[PtCl(NH_3)_2(L)]^+ + H_2O$ ligand substitution reaction examined in FT-ICR mass spectrometry. Overall, the following reactivity trend is observed: trimethylphosphate>4(5)-methylimidazole, thioanisole>pyridine. Interestingly, although the TMP reaction is the least exothermic (Figure 7), the comparatively fast kinetics may suggest a cisplatin 'carrier' role for this specimen of a functional group ubiquitous in the biological environment.[29] The computational inquiry has also yielded a value for the proton affinity of *cis*-$[PtCl(NH_3)_2(OH)]$ equal to 964 kJ mol^{-1}, which may be compared with the proton affinity of 831 kJ mol^{-1} for cisplatin undergoing protonation on chlorine.[30]

It should be underlined that all reported data refer to charged species isolated in the gas phase, an environment very different from the biological medium where cisplatin-derived intermediates are acting. The gaseous environment is expected, however, to provide a reference condition allowing to better understand

the role of other factors, such as the dielectric constant, on the reactivity and selectivity in the reactions of metal complexes with biomolecules.[31] The present study has focused on the formation of *cis*-$[PtCl(NH_3)_2(L)]^+$ that are representative monofunctional platinum(II) agents, namely compounds exhibiting interaction with DNA and potential chemotherapeutic and medicinal inorganic chemistry applications.[32] Forthcoming inquiry is planned to address biomolecular targets of increasing size and functional relevance.

Supporting Information available: Experimental procedures, mass spectra, IRMPD and calculated IR spectra along with calculated structures and energies including Cartesian coordinates of all theoretically studied species.

Acknowledgements

Support from the Università degli Studi di Roma "La Sapienza" is gratefully acknowledged. The IRMPD work in the fingerprint range was supported by the European Commission (CLIO project IC14-011) We thank Philippe Maitre, Jean-Michel Ortega and Vincent Steinmetz, and the CLIO team and are grateful to Annito Di Marzio for experiments at the OPO/OPA laser.

Keywords: ligand substitution reaction, structure elucidation, ion-molecule reactions, ESI mass spectrometry, bioinorganic chemistry

References

[1] a) B. Rosenberg, L. VanCamp, T. Krigas, *Nature* **1965**, *205*, 698; b) B. Rosenberg, L. VanCamp, J. E. Trosko, V. H. Mansour, *Nature* **1969**, *222*, 385.

[2] a) S. M. Cohen, S. J. Lippard, *Prog. Nucleic Acid Res. Mol. Biol.* **2001**, *67*, 93; b) J. Reedijk, *Pure Appl. Chem.* **1987**, *59*, 181.

[3] B. P. Esposito, R. Najjar, *Coord. Chem. Rev.* **2002**, *232*, 137.

[4] a) A. Casini, J. Reedijk, *Chem. Sci.* **2012**, *3*, 3135; b) M. A. Fuertes, C. Alonso, J. M. Pérez, *Chem. Rev.* **2003**, *103*, 645.

[5] a) S. E. Miller, K. J. Gerard, D. A. House, *Inorg. Chim. Acta* **1991**, *190*, 135; b) K. Hindmarsh, D. A. House, M. M. Tumbull, *Inorg. Chim. Acta* **1997**, *257*, 11; c) J. Arpalahti, M. Mikola, S. Mauristo, *Inorg. Chem.* **1993**, *32*, 3327; d) M. Mikola, J.Arpalahti, *Inorg. Chem.* **1994**, *33*, 4439; e) J.-L. Jestin, B. Lambert, J.-C. Chottard, *J. Biol. Inorg. Chem.* **1998**, *3*, 515.

[6] a) L. A. S. Costa, W. R. Rocha, W. B. De Almeida, H. F. Dos Santos, *J. Chem. Phys.* **2003**, *118*, 10584; b) L. A. S. Costa, W. R. Rocha, W. B. De Almeida, H. F. Dos Santos, *Chem. Phys. Lett.* **2004**, *387*, 182; c) A. Robertazzi, J. A. Platts, *J. Comput. Chem.* **2004**, *25*, 1060; d) L. A. S. Costa, W. R. Rocha, W. B. De Almeida, H. F. Dos Santos, *J. Inorg. Biochem.* **2005**, *99*, 575; e) J. Burda, M. Zeizinger, J. Leszczynski, *J. Comput. Chem.* **2005**, *26*, 914; f) P. Carloni, M. Sprik, W. Andreoni, *J. Phys. Chem. B* **2000**, *104*, 823; g) J. K.-C. Lau, D. V. Deubel, *J. Chem. Theory Comput.* **2006**, *2*, 103; h) J. V. Burda, M. Zeizinger, J. Leszczynski, *J. Chem. Phys.* **2004**, *120*, 1253; i) Y. Zhang, Z. Guo, X.-Z. You, *J. Am. Chem. Soc.* **2001**, *123*, 9378.

[7] a) M. Cui, Z. Mester, *Rapid Commun. Mass Spectrom.* **2003**, *17*, 1517; b) A. Springer, C. Buergel, V. Boehrsch, R. Mitric, V. Bonacic-Koutecky, M. W. Linscheid, *ChemPhysChem* **2006**, *7*, 1779.

[8] a) D. Yonggang, N. Zhang, M. Cui, Z. Liu, S. Liu, *Rapid Commun. Mass Spectrom.* **2012**, *26*, 2832; b) Z. Xu, J. B. Shaw, J. S. Brodbelt, *J. Am. Soc. Mass Spectrom.* **2013**, *24*, 265.

[9] a) H. Schwarz, *Israel J. Chem.* **2014**, *54*, 1413; b) B. Butschke, H. Schwarz, *Chem. Eur. J.* **2012**, *18*, 14055; c) M. Schlangen, H. Schwarz, *Dalton Trans.* **2009**, 10155; d) D. Schröder, H. Schwarz, *Proc. Natl. Acad. Sci.* USA **2008**, *105*, 18114; e) D. K. Bohme, H. Schwarz, *Angew. Chem.*

Int. Ed. **2005**, *44*, 2336; f) M.-E. Moret, P. Chen, *Organometallics* **2007**, *26*, 1523; g) P. B. Armentrout, *Int. J. Mass Spectrom.* **2003**, *227*, 289.

[10] a) J. Oomens, B. G. Sartakov, G. Meijer, G. von Helden, *Int. J. Mass Spectrom.* **2006**, *254*, 1; b) L. MacAleese, P. Maitre, *Mass Spectrom. Rev.* **2007**, *26*, 83; c) J. R. Eyler, *Mass Spectrom. Rev.* **2009**, *28*, 448; d) T. D. Fridgen, *Mass Spectrom. Rev.* **2009**, *28*, 586; e) T. Baer, R. C. Dunbar, *J. Am. Soc. Mass Spectrom.* 2010, *21*, 681; f) N. C. Polfer, *Chem. Soc. Rev.* **2011**, *40*, 2211; g) J. Roithova, *Chem. Soc. Rev.* **2011**, *41*, 547; h) E. Kleisath, R. A. Marta, S. Martens, J. Martens, T. McMahon, *J. Phys. Chem. A* **2015**, *119*, 6689.

[11] A. De Petris, A. Ciavardini, C. Coletti, N. Re, B. Chiavarino, M. E. Crestoni, S. Fornarini, *J. Phys. Chem. Lett.* **2013**, *4*, 3631.

[12] B. Chiavarino, M. E. Crestoni, S. Fornarini, D. Scuderi, J.-Y. Salpin, *J. Am. Chem. Soc.* **2013**, *135*, 1445.

[13] B. Chiavarino, M. E. Crestoni, S. Fornarini, D. Scuderi, J.-Y. Salpin, *Inorg. Chem.* **2015**, *54*, 3513.

[14] G. S. Li, M. F. Ruiz-Lopez, B. Maigret, *J. Phys. Chem. A* **1997**, *101*, 7885.

[15] a) Z. D. Bugarcic, J. Bogojeski, R. van Eldik, *Coord. Chem. Rev.* **2015**, *292*, 91; b) T. G. Appleton, Coord. Chem. Rev. 1997, 166, 313; c) A. Casini, J. Reedijk, *Chem. Sci.* **2012**, *3*, 3135; d) G. Ferraro, L. Massai, L. Messori, A. Merlino, *Chem. Commun.* **2015**, *51*, 9436; e) A. R. Timerbaev, C. G. Hartinger, S. S. Aleksenko, B. K. Keppler, *Chem. Rev.* **2006**, *106*, 2224; f) H. Li, Y. Zhao, H. I. A. Phillips, Y. Qi, T.-Y. Lin, P. J. Sadler, P. B. O'Connor, *Anal. Chem.* **2011**, *83*, 5369; g) L. Feketeova, V. Ryzhov, R. A. J. O'Hair, *Rapid Comm. Mass Spectrom.* **2009**, *23*, 3133; h) R. A. J. O'Hair, *Eur. J. Mass Spectrom.* **1997**, *3*, 390; and references therein.

[16] a) A. R. Battle, J. A. Platts, T. W. Hambley , G. B. Deacon, *J. Chem. Soc. Dalton Trans.* **2002**, 1898; b) J. Kozelka, G. Barre, *Chem. Eur. J.* **1997**, *3*, 1405; c) T. G. Appleton, R. D. Berry, C. A. Davis, J. R. Hall, H. A. Kimlin, *Inorg. Chem.* **1984**, *23*, 3514; d) R. N. Bose, N. Goswami, S. Moghaddas, *Inorg. Chem.* **1990**, *29*, 3461.

[17] a) D. T. Richens, Chem. Rev. 2005, 105, 1961; b) M. Eigen, Pure Appl. Chem. 1963, 6, 97; c) C. E. Housecroft, A. G. Sharpe, *Inorganic Chemistry* 2nd edition, Pearson Education Ltd, Harlow, UK, **2005**, p. 772; d) J. Burgess, *Ions in Solution. Basic Principles of Chemical Interactions* 2nd edition, Woodhead Publishing Ltd, Cambridge, UK, **2011**, p. 125.

[18] a) M. A. Sainna, S. Kumar, D. Kumar, S. Fornarini, M. E. Crestoni, S. de Visser, *Chem. Sci.* **2015**, *6*, 1516; b) S. Osburn, V. Ryzhov, *Anal. Chem.* **2013**, *85*,769.

[19] Z. D. Bugarcic, J. Bogojeski, B. Petrovic, S. Hochreuther, R. van Eldik, *Dalton Trans.***2012**, *41*, 12329.

[20] a) J. Lemaire, P. Boissel, M. Heninger, G. Mauclaire, G. Bellec, H. Mestdagh, A. Simon, S. Le Caer, J. M. Ortega, F. Glotin, P. Maitre, *Phys. Rev. Lett.* **2002**, *89*, 273002; b) J. M. Bakker, T. Besson, J. Lemaire, D. Scuderi, P. Maitre, *J. Phys. Chem. A* **2007**, *111*, 13415 ; c) B. Chiavarino, M. E. Crestoni, S. Fornarini, F. Lanucara, J. Lemaire, P. Maitre, D. Scuderi, *ChemPhysChem* **2008**, *9*, 826.

[21] a) D. T. Moore, J. Oomens, J. R. Eyler, G. von Helden, G. Meijer, R. C. Dunbar, *J. Am. Chem. Soc.* **2005**, *127*,7243; b) R. K. Sinha, B. Chiavarino, S. Fornarini, J. Lemaire, P. Maitre, M. E. Crestoni, *J. Phys. Chem. Lett.* **2010**, *1*, 1721.

[22] a) S. Wee, R. A. J. O'Hair, W. D. McFadyen, *Rapid Comm. Mass Spectrom.* **2004**, *18*, 1221; b) W. K. C. Lo, G. Cavigliasso, R. Stranger, J. D. Crowley, A. G. Blackman, *Inorg. Chem.* **2014**, *53*, 3595; and references therein.

[23] a) J. Bergès, I. Fourré, J. Pilmé, J. Kozelka, *Inorg. Chem.* **2013**, *52*, 1217; b) F. Jalilehvand, L. J. Laffin, *Inorg. Chem.* **2008**, *47*, 3248; c) L. Kocsis, J. Mink, F. Jalilehvand, L. J. Laffin, O. Berkesi , L. Hajba, *J. Raman Spectr.* **2009**, *40*, 481; d) R. Sanchez-de-Armas, M. S. G. Ahlquist, *Phys. Chem. Chem. Phys.* **2015**, *17*, 812; e) M. Baya, U. Belio, A. Martin, *Inorg. Chem.* **2014**, *53*, 189; f) J. Kozelka, J. Berges, R. Attias, J. Fraitag, *Angew. Chem. Int. Ed.* **2000**, *39*, 198.

[24] E. P. Hunter, S. G. Lias, in Proton Affinity Evaluation in NIST Chemistry WebBook, ed. P.J. Linstrom and W.G. Mallard, National Institute of Standards and Technology, MD, 20899, http://webbook.nist.gov, NIST Standard Reference Database Number 69.

[25] a) R. K. Sinha, P. Maitre, S. Piccirillo, B. Chiavarino, M. E. Crestoni, S. Fornarini, *Phys. Chem. Chem. Phys.* **2010**, *12*, 9794; b) A. Filippi, C. Fraschetti, S. Piccirillo, F. Rondino, B. Botta, I. D'Acquarica, A. Calcaterra, M. Speranza, *Chem. Eur. J.* **2012**, *18*, 8320.

[26] a) S. M. Hamilton, W. S. Hopkins, D. J. Harding, T. R. Walsh, M. Haertelt, C. Kerpal, P. Gruene, G. Meijer, A. Fielicke, S. R. MacKenzie, *J. Phys. Chem. A* **2011**, *115*, 2489; b) D. J. Harding, A. Fielicke, *Chem. Eur. J.* **2014**, *20*, 3258.
[27] a) M. L. Chabinyc, S. L. Craig, C. K. Regan, J. I. Brauman, *Science* **1998**, *279*, 1882; b) W. N. Olmstead, J. I. Brauman, *J. Am. Chem. Soc.* **1977**, *99*, 4219; c) S. Gronert, *Chem. Rev.* **2001**, *101*, 329.
[28] a) A. Ciancetta, C. Coletti, A. Marrone, N. Re, *Dalton Trans.* **2012**, 41, 12960; b) P.N.V. Pavankumar, P.Y. Ayala, A.R. Parker, M. Zhao, K. Jair, X. Chen, H. Kochat, F. H. Hausheer, *J. Phys. Chem. Biophys.* **2014**, *4*, 1000163.
[29] M. S. Davies, S. J. Berners-Price, T. W. Hambley, *Inorg. Chem.* **2000**, *39*, 5603.
[30] M. Juhasz, S. Takahashi, S. Arulmozhiraja, T. Fujii, *J. Struct. Chem.* **2012**, *53*, 436.
[31] D. V. Deubel, *J. Am. Chem. Soc.* **2004**, *126*, 5999.
[32] a) T. C. Johnstone, J. J. Wilson, S. J. Lippard, *Inorg. Chem.* **2013**, *52*, 12234; b) T. C. Johnstone, S. M. Alexander, W. Lin, S. J. Lippard, *J. Am. Chem. Soc.* **2014**, *136*, 116.

Graphical abstract

An Eigen-Wilkins encounter complex in the reactant preassociation mechanism for ligand substitution in solution is directly identified by electrospray ionization-mass spectrometry. Key intermediates and reactive events accounting for cisplatin activity are elucidated in a controlled environment, the gas phase, with unprecedented detail.